

Thaer M. Al-Jadir, and Flor R. Siperstein

\*E-mail: [150046@uotechnology.edu.iq](mailto:150046@uotechnology.edu.iq)

<https://doi.org/10.1016/j.micromeso.2018.06.002>

Microporous and Mesoporous Materials

Volume 271, 15 November 2018, Pages 160-168

## Molecular Simulations of Metal-Organic Frameworks for Acid Gas Adsorption

### The influence of the pore size in Metal–Organic Frameworks in adsorption and separation of hydrogen sulphide: a molecular simulation study

Thaer M. Al-Jadir <sup>\*,a,b</sup> and Flor R. Siperstein <sup>a</sup>

<sup>a</sup> School of Chemical Engineering and Analytical Science, University of Manchester, M13 9PL, U.K

<sup>b</sup> Environmental Research Center, University of Technology- Iraq, Baghdad, Iraq.

\*E-mail: [150046@uotechnology.edu.iq](mailto:150046@uotechnology.edu.iq)

#### 1. What are Metal-Organic Frameworks (MOFs) and how do they work as adsorbents in industrial separations?

- Metal-Organic Frameworks (MOFs) have the potential to be used as adsorbents in industrial separations. MOFs are materials composed of metal ions or clusters linked by organic ligands to form a porous structure with high surface area and tunable pore size. They work as adsorbents by selectively capturing and separating molecules based on their size, shape, and chemical properties. The unique properties of MOFs make them promising candidates for various applications, including gas storage, catalysis, drug delivery, and environmental remediation.

#### 2. How do ligand lengths affect the pore size of MOFs, and how does this impact their ability to adsorb H<sub>2</sub>S and CH<sub>4</sub>?

- Different ligand lengths can generate MOFs with similar topology but differing pore sizes. The impact of the linker on the macroscopic properties of MOFs is negligible at low pressures, but it becomes evident at high pressures, where adsorption far from the linker is observed in large pore materials. In this study, molecular simulations were used to assess the adsorption isotherms, heats of adsorption and selectivity of H<sub>2</sub>S and CH<sub>4</sub> in MOF UiO-66, UiO-67, and UiO-68. Based on the adsorption selection parameter, UiO-67 shows better performance in a wider range of conditions than the other materials. Therefore, it appears that ligand lengths can affect the pore size and ultimately impact the ability of MOFs to adsorb specific molecules such as H<sub>2</sub>S and CH<sub>4</sub>.

#### 3. What insights were gained from the molecular simulations used in this study, and how can they inform the development of more effective adsorbents for acid gases?

- The molecular simulations used in this study provided insights into the adsorption isotherms, heats of adsorption, and selectivity of H<sub>2</sub>S and CH<sub>4</sub> in MOF UiO-66, UiO-67, and UiO-68. The detailed analysis of the distribution of molecules in the cages and the radial distribution functions suggest that the effect of the linker on the macroscopic properties is negligible at low pressures, but it becomes evident at high pressures. Based on the adsorption selection parameter, UiO-67 shows better performance in a wider range of conditions than the other materials. These insights can inform the development of more effective adsorbents for acid gases by providing a better understanding of how MOFs work and how their properties can be optimized for specific applications. By designing MOFs with tailored pore sizes and chemical functionalities, it may be possible to develop more efficient and selective adsorbents for acid gases that could have important industrial applications.

Thaer M. Al-Jadir, and Flor R. Siperstein

\*E-mail: [150046@uotechnology.edu.iq](mailto:150046@uotechnology.edu.iq)

<https://doi.org/10.1016/j.micromeso.2018.06.002>

Microporous and Mesoporous Materials

Volume 271, 15 November 2018, Pages 160-168

## Abstract

Metal Organic Frameworks (MOFs) have the potential to be used as adsorbents in industrial separations. Different ligand lengths can generate MOFs with similar topology but differing pore sizes. Molecular simulations were used in this work to assess the adsorption isotherms, heats of adsorption and selectivity of H<sub>2</sub>S and CH<sub>4</sub> in MOF UiO-66, UiO-67, and UiO-68. Detailed analysis of the distribution of molecules in the cages and the radial distribution functions suggest that the effect of the linker on the macroscopic properties is negligible at low pressures, but it becomes evident at high pressures, where adsorption far from the linker is observed in large pore materials. Based on the adsorption selection parameter, UiO-67 shows better performance in a wider range of conditions than the other materials.

## Introduction

The composition of natural gas varies substantially depending on the source, but mainly consists of methane, ethane, propane, butane, pentane, and hexane. Natural gas also contains undesirable impurities, such as water, carbon dioxide, hydrogen sulphide and nitrogen. If the hydrogen sulphide (H<sub>2</sub>S) content is greater than 5.7 mg/m<sup>3</sup> at standard pressure and temperature, it is called sour natural gas [1][2]. Hydrogen sulphide is a highly toxic, corrosive gas, with a strong offensive odor [3]. Therefore, the separation of the hydrogen sulphide is of economic and environmental importance for the efficient utilization of natural gas. The elimination of hydrogen sulphide can be performed by adsorption, physical or chemical absorption, biological processes, cryogenic and membrane permeation or conversion by metal oxides [2].

Adsorption is a low energy technology, especially when compared with liquid absorption processes [4], it is non-toxic in comparison to ionic liquids [5][6], not prone to problems with corrosion when compared with chemical absorption [7], and is a robust and proven technology for gas separations compared with membrane permeation which can be seriously damaged by free liquids. Moreover, the life of the membranes does not go over 3 to 4 years [8] and membrane based on polymers are not selective enough for H<sub>2</sub>S–CH<sub>4</sub> mixtures [9]. Alternatively, pressure swing adsorption (PSA) selectively removes hydrogen sulphide, but its performance is highly dependent on the choice of adsorbent. Therefore, the development of novel adsorbents with a larger capacity and selectivity is an active area of research.

Several types of adsorbents such as metal oxides, activated carbons, zeolites and metal–organic frameworks (MOFs) have been reported in the literature for adsorption of hydrogen sulphide [10][11][12][13][14][15][16]. Activated carbon is composed largely of neutral atoms of a single species, with no significant potential gradients to attract and orient polar molecules in preference to nonpolar molecules [17]. The functional groups present in the material as a result of the activation process may provide some preferential adsorption sites for polar molecules [18], but often they are not sufficient to result in a highly selective material. Consequently, activated carbon tends to adsorb all gases roughly in proportion to their concentrations [17]. Zeolites, activated aluminas and silica gels have high selectivity for polar gases. However, in the presence of moisture these adsorbents can become ineffective due to the relatively large amount of water that can adsorbed [10] [17][19]. MOFs can be constructed to preferentially adsorb polar molecules without being affected by moisture [20].

The main advantage of MOFs over more conventional porous materials, such as zeolites and activated carbon, is the greater possibility for tailoring these materials for specific applications. This is because MOFs are constructed with two major components: a metal ion or a cluster of metal ions and an organic

Thaer M. Al-Jadir, and Flor R. Siperstein

\*E-mail: [150046@uotechnology.edu.iq](mailto:150046@uotechnology.edu.iq)

<https://doi.org/10.1016/j.micromeso.2018.06.002>

Microporous and Mesoporous Materials

Volume 271, 15 November 2018, Pages 160-168

molecule called a linker as shown schematically in Figure 1a. By tuning the length of the organic linker and changing or mixing the metal ion thus, the diversity of MOF materials is nearly infinite [21]. A systematic molecular simulation study for adsorption and separation of hydrogen sulphide was performed in this work to investigate the effect of pore size in a range of Zr-MOFs (see Figure 1b), a class of MOFs in which all members have the same topology cages and the same corner units.

### Simulation Method

UiO-66, UiO-67 and UiO-68 were first synthesized by Cavka *et al.* 2008 [22]. The hydroxylated forms of these analogue materials are built up from the inorganic block  $Zr_6$ -octahedra [ $Zr_6O_4(OH)_4$ ] bounded to twelve organic linkers, leading to a three-dimensional arrangement of micropores with each centric octahedral cage surrounded by eight corner tetrahedral cages through triangular windows Figure 1c.

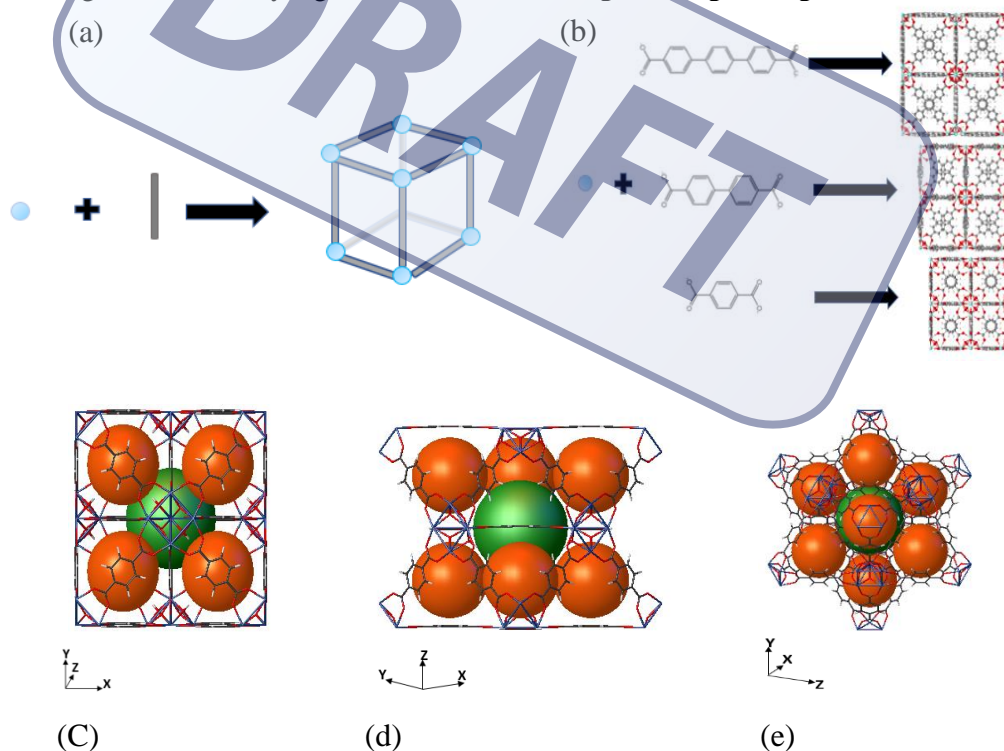


Figure 1. (a) Schematic representation for the construction of MOFs. (b) Building blocks and the resulting extended 3D network of different Zr-MOFs used in this work: UiO-66, UiO-67 and UiO-68 (zirconium, light blue; carbon, grey; oxygen, red; hydrogen, white). (c), (d) and (e) show the octahedral cage (green sphere) and tetrahedral cages (orange spheres) in UiO-66 (Zr).

Zr-MOFs are thermostable, have a high working capacity, low-cost regenerability, can withstand humid acid gas conditions, remaining stable after exposure to conditions of high humidity and mechanical pressure [23][24][25][20]. The Zr-MOFs family used in this study have linkers of different lengths, but are chemically similar, with pore size being the main difference between them allowing the effect of pore size to be considered separately from the effect of the chemical composition of the materials and

Thaer M. Al-Jadir, and Flor R. Siperstein

\*E-mail: [150046@uotechnology.edu.iq](mailto:150046@uotechnology.edu.iq)

<https://doi.org/10.1016/j.micromeso.2018.06.002>

Microporous and Mesoporous Materials

Volume 271, 15 November 2018, Pages 160-168

metal cluster in the adsorption and separation of hydrogen sulphide. The properties of these materials are summarized in Table 1.

TABLE 1: Properties of the Zr-MOFs materials investigated

Materials	Linker	$\rho_{\text{cyrst}}^{\text{a}}$ (g cm <sup>-3</sup> )	$V_{\text{pore}}^{\text{a}}$ (cm <sup>3</sup> g <sup>-1</sup> )	$\rho_{\text{cyrst}}^{\text{b}}$ (g cm <sup>-3</sup> )	$V_{\text{pore}}^{\text{b}}$ (cm <sup>3</sup> g <sup>-1</sup> )	Pore limiting diameter <sup>b</sup> (Å)	Maximum pore diameter <sup>b</sup> (Å)
UIO-66	BDC	1.197	0.45	1.193	0.458	3.82	8.03
UIO-67	BPDC	0.708	1.05	0.641	1.114	5.49	13.09
UIO-68	TPDC	0.462	1.82	0.435	1.857	9.70	17.15

<sup>a</sup> From reference [26];

<sup>b</sup> Obtained by Poreblazer, developed by: Lev Sarkisov, 2012 [27];

**Simulation Details.** The equilibrium between the bulk gas phase and the adsorbed phase was modeled using grand canonical Monte Carlo (GCMC) simulations as implemented in Towhee [28]. Detailed descriptions of GCMC simulations are given in several references [28][29][30][31]. In the grand canonical ensemble, the chemical potential of each component, the temperature, and the volume are kept constant as in adsorption experiments. The chemical potential  $\mu$  required in the GCMC simulation was obtained from independent isobaric–isothermal ensemble *NPT* simulations; the chemical potentials are given in Tables S1 and S2. An atomistic model was used for the MOFs, in which the framework atoms were kept fixed at the crystallographic positions thereby ignoring the skeleton stretching and bending vibration as these materials do not show any gate opening or breathing effects. The crystallographic data of the framework atoms were taken from Yang *et al.* [26]. The number of unit cells in the simulation box is  $1 \times 1 \times 1$ . Interactions beyond 10 Å were neglected. Although it is small cutoff, compared with what is commonly used [16] [26], the difference in the amounts adsorbed using the different cutoffs is negligible, and it allowed us to use relatively small simulation boxes (see Figure S1 supporting information). The long-range electrostatic interactions were calculated by the Ewald summation technique to have a reasonable convergence and computational effort [31][32].

The van der Waals interactions between the sorbate molecules themselves, as well as between the sorbate molecules and the Zr-MOFs, were described with a 12–6 Lennard-Jones (LJ) potential. The Lorentz-Berthelot mixing rules were used to calculate mixed Lennard-Jones parameters. The parameters for the framework atoms were obtained from DREIDING [33] and UFF [34] force field and partial charges were adopted from the work of Yang *et al.* 2012 [26]. The parameters for the framework atoms are reported in Table S3. The use of these potentials in the simulation of MOFs has been validated in previous studies [16] [26].

Hydrogen sulphide was represented by three interaction sites reported by Kamath *et al.*[35], such a model has been successfully used to reproduce the experimental vapor–liquid phase equilibrium data and is in good agreement with the experimental isotherm of adsorption hydrogen sulphide on UiO-66 [16]. This strongly suggests that these force fields are suitable for modelling the adsorption of H<sub>2</sub>S on UiO-67 and UiO-68 for which experimental adsorption isotherms have not yet been measured.

Methane was represented by one-site model using the TraPPE-UA [36] force field, a model which has shown quantitative agreement between experimentally measured and simulated methane isotherms in

Thaer M. Al-Jadir, and Flor R. Siperstein

\*E-mail: [150046@uotechnology.edu.iq](mailto:150046@uotechnology.edu.iq)

<https://doi.org/10.1016/j.micromeso.2018.06.002>

Microporous and Mesoporous Materials

Volume 271, 15 November 2018, Pages 160-168

UiO-66 and has been used to predict adsorption isotherms for UiO-67 and UiO-68 [16] [26]. The parameters for hydrogen sulphide and methane are reported in Table S4.

GCMC simulations of the pure gas adsorption isotherms carried out at  $T = 303$  K, with  $2 \times 10^7$  steps to ensure equilibration, followed by  $2 \times 10^7$  steps to sample the desired thermodynamic properties.

The selectivity of  $H_2S$  over  $CH_4$  was calculated from mixture simulations at two different bulk gas compositions: 5% and 18.8%, which correspond to the range of concentrations found in natural gas [37]. GCMC simulation of the mixtures carried out at  $T = 303$  K, with  $5 \times 10^7$  steps to ensure the equilibration, followed by  $2 \times 10^7$  steps to sample the desired thermodynamic properties. The frequency of translation, rotation, and insertion or deletion moves was 10%, 20%, and 70%, respectively. The heat of adsorption for pure components was calculated using the fluctuations in energy and number of molecules [38]:

$$Q_{st} = RT - \frac{\langle UN \rangle - \langle U \rangle \langle N \rangle}{\langle N^2 \rangle - \langle N \rangle^2} \quad (1)$$

where  $Q_{st}$  is the heat of adsorption,  $R$  is the gas constant,  $T$  is the temperature,  $U$  is the energy, and  $N$  is the number of particles adsorbed. The brackets represent an ensemble average.

The selectivity of the adsorbent,  $\alpha_{ij}$ , for component  $i$  relative to component  $j$  is

$$\alpha_{ij} = \frac{n_i/p_i}{n_j/p_j} \quad (2)$$

where  $n_i$  is the number of adsorbed molecules of type  $i$  and  $p_i$  is the partial pressure of component  $i$ .

For pressure swing adsorption process, the evaluation of a suitable sorbent for a given separation is a complex problem. The adsorbent selection parameter  $S$  defined in equation (3) is a simple tool to identify suitable adsorbents because it includes the ratio of adsorption capacity for both components as well as the selectivity [39][40].

$$S = \frac{\Delta q_i}{\Delta q_j} \alpha_{ij} \quad (3)$$

In equation (3),  $\Delta q_i$  and  $\Delta q_j$  are the working capacities for each component, that are calculated as the difference between the equilibrium amount adsorbed at high pressure (2 MPa) and low pressure (0.01 MPa) for components  $i$  and  $j$ , respectively.

## Results and Discussion

Figure 2 shows simulated isotherms for hydrogen sulphide on UiO-66, UiO-67 and UiO-68. The fitted pure-component isotherm parameters to the dual Langmuir-Freundlich and dual Langmuir models are provided in the Supporting Information (Figure S3 and Tables S5 and S6). Good agreement was obtained between the simulated adsorption isotherms in UiO-66 and those in the literature [16].

The pure component isotherms of hydrogen sulphide are shown in Figure 2a and those for methane are shown in Figure 3a. As expected, the adsorbent capacity increases with increasing pore size for both gases, but in the case of methane, the shape of the adsorption isotherm is the same regardless of the pore size, but the pore size affects the adsorption isotherm shape of  $H_2S$ : in UiO-66 shows a type I isotherm according to the IUPAC classification, while the type IV shape is more obvious for UiO-68 than for UiO-67. The inflection point in the isotherm is evident when plotting the isotherm slope or a

Thaer M. Al-Jadir, and Flor R. Siperstein

\*E-mail: [150046@uotechnology.edu.iq](mailto:150046@uotechnology.edu.iq)

<https://doi.org/10.1016/j.micromeso.2018.06.002>

Microporous and Mesoporous Materials

Volume 271, 15 November 2018, Pages 160-168

$P/n$  vs  $n$  curve (see Supporting Information). This is considered a consequence of relatively weak adsorbent-adsorbate interactions, the interactions decrease with increasing pore size and the isotherm shape transitions to type I by increasing the temperature [21] [41]. This transition takes place at approximately 350 K for both UiO-67 and UiO-68 MOFs (adsorption isotherms at high temperatures are shown in the Supporting Information).

The isosteric heats of adsorption in Figure 2b show a slight increase with coverage. In general, the isosteric heat of adsorption are constant if the surface is energetically homogeneous, increase due to lateral interactions between adsorbed molecules, and decrease due to surface heterogeneity [42] [43][44]. In the cases studied, the lateral interactions dominate over any surface heterogeneity, especially for large pore size materials. Heats of adsorption for methane in Figure 3b.

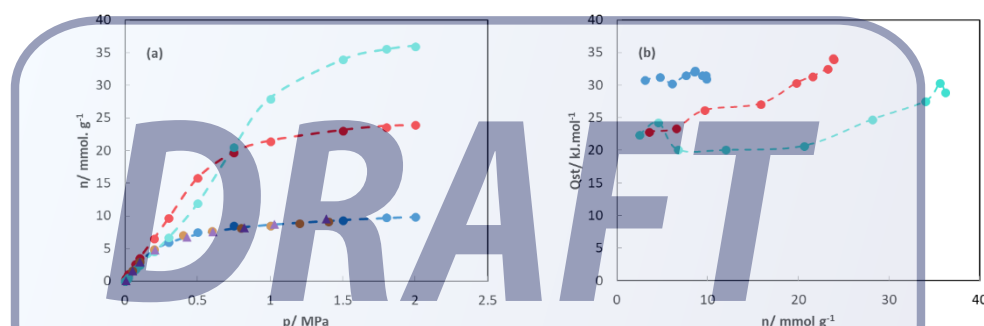


Figure 2. Hydrogen sulphide (a) adsorption isotherms and (b) heats of adsorption at 303 K in UiO-66 (blue), UiO-67 (red) and UiO-68 (turquoise) MOFs calculated in this work. Experimentally measured (purple triangles) and calculated (orange circles) adsorption isotherms as reported by Li, et al. [16] are shown for comparison. The dashed lines represent the dual Langmuir-Freundlich fitted curves. The statistical uncertainty of the calculated loading is smaller than the symbol size.

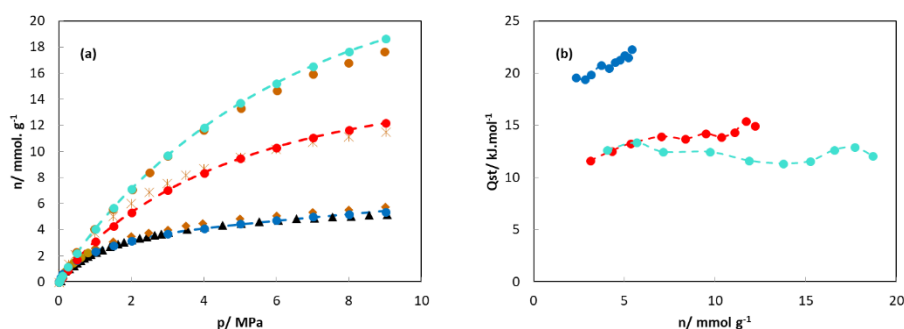


Figure 3. Methane (a) adsorption isotherms and (b) heats of adsorption at 303 K in UiO-66 (blue), UiO-67 (red) and UiO-68 (turquoise) MOFs calculated in this work. Experimental data (black triangles) and molecular simulation results UiO-66 (orange diamonds), UiO-67 (orange crosses) and UiO-68 (orange circles) reported in the literature [26] are shown for comparison. The dashed lines represent the dual Langmuir-Freundlich fitted curves. The statistical uncertainty of the calculated loading is smaller than the symbol size.

The selectivity of H<sub>2</sub>S over CH<sub>4</sub> shown in Figure 4 was calculated from mixture simulations at two different bulk gas compositions: 5% and 18.8%. The selectivities for UiO-66 and UiO-67 are similar

Thaer M. Al-Jadir, and Flor R. Siperstein

\*E-mail: [150046@uotechnology.edu.iq](mailto:150046@uotechnology.edu.iq)

<https://doi.org/10.1016/j.micromeso.2018.06.002>

Microporous and Mesoporous Materials

Volume 271, 15 November 2018, Pages 160-168

especially at low loadings. UiO-67 shows slightly larger selectivity than UiO-66 at low gas phase compositions of H<sub>2</sub>S, but the difference disappears as the gas phase concentration increases. UiO-68 shows clearly lower selectivity, which can be attributed to the larger pore sizes and lower degree of confinement of the molecules. It is interesting to note that the selectivity tends to increase with pressure, which is counterintuitive for many adsorbents where the surface-fluid interactions dominate the material's behavior, but similar to what has been reported in UiO-66 [16]. In this case, the ability of the H<sub>2</sub>S molecules to pack better due to their small size can result in an increase in selectivity with pressure. The formation of a hydrogen bond network between adsorbed H<sub>2</sub>S molecules may also contribute to the increase in selectivity with pressure, nevertheless, radial distribution functions for adsorbed H<sub>2</sub>S molecules (see Figure S11 and Figure S15) suggest that they are too far apart to form a network. The adsorbent selection parameters,  $S_{ij}$ , in Table 2 were calculated using equation 3 considering the low pressure as 0.01 MPa, and the high pressure as 2 MPa. The selectivity,  $\alpha_{ij}$ , was taken as the average selectivity between these pressures. The trends in the adsorption selection parameters are similar to those observed in the difference of heats of adsorption between the two gases [15][16], which in this work correspond to: 12.3 kJ/mol in UiO-66, 13.1 kJ/mol in UiO-67 and 7.4 kJ/mol in UiO-68.

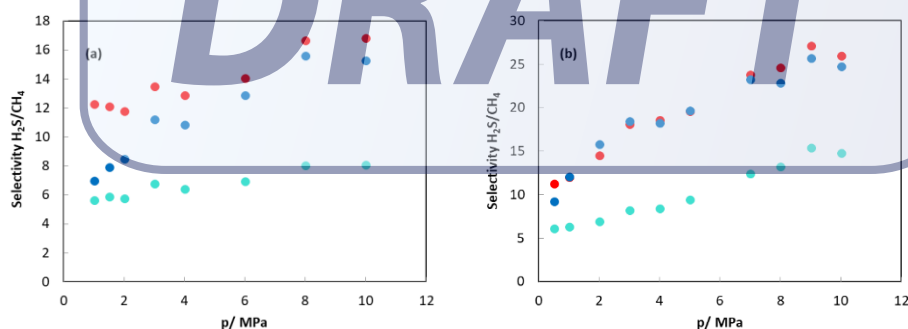


Figure 4. Selectivity of hydrogen sulphide over methane as a function of pressure on UiO-66 (blue), UiO-67 (red) and UiO-68 (turquoise) for (a)  $y_{\text{H}_2\text{S}} = 0.05$  and (b)  $y_{\text{H}_2\text{S}} = 0.188$ .

Table 2. Average selectivity and adsorbent selection parameters for an adsorption pressure of 2 MPa and a desorption pressure of 0.01 MPa.

H <sub>2</sub> S mole fraction	$\alpha_{ij}$			$S_{ij}$		
	UiO-66	UiO-67	UiO-68	UiO-66	UiO-67	UiO-68
0.050	10.5	18.8	6.8	18.6	36.0	13.0
0.188	15.9	21.3	10.8	28.3	40.8	20.8

Agreement between the experimentally measured properties and those calculated from the simulations provides confidence in the models selected to then analyze the microscopic structure of the system. Figure 5 shows the location of adsorbed molecules during the simulation. At low pressure, hydrogen sulphide molecules are preferentially adsorbed in the tetrahedral cages, and as the pressure increases, the octahedral cages start to be populated. The required pressure to start populating the octahedral cages increases with increasing pore size. At high pressures, such as 2 MPa, H<sub>2</sub>S molecules fill the whole void volume of the MOF. The pressure at which the octahedral cage starts to be populated increases with increasing the linker length.

Thaer M. Al-Jadir, and Flor R. Siperstein

\*E-mail: [150046@uotechnology.edu.iq](mailto:150046@uotechnology.edu.iq)

<https://doi.org/10.1016/j.micromeso.2018.06.002>

Microporous and Mesoporous Materials

Volume 271, 15 November 2018, Pages 160-168

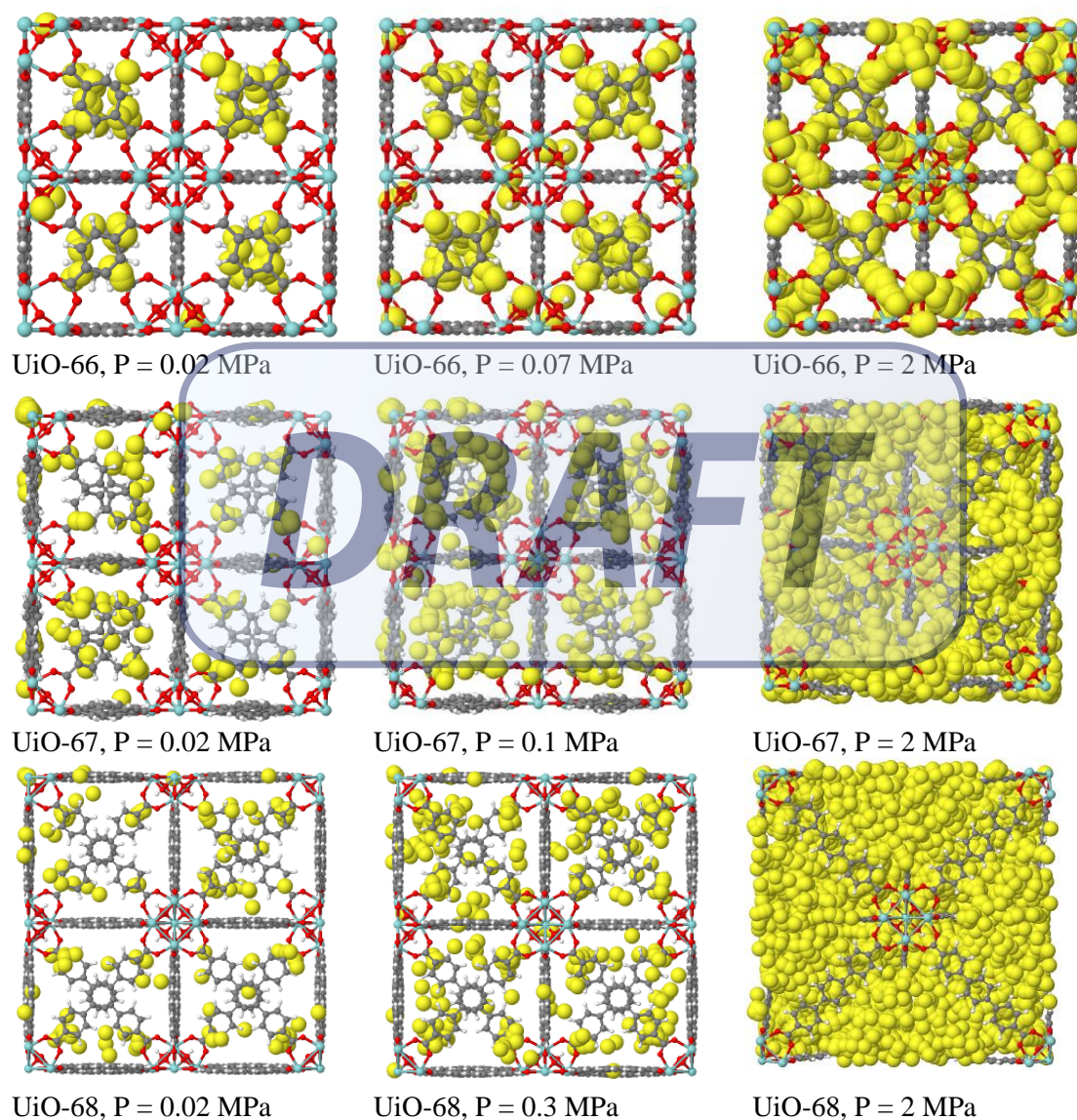


Figure 5. Location of H<sub>2</sub>S molecules in UiO MOFs at different pressures and 303 K. The positions of H<sub>2</sub>S molecules during the simulation are shown as yellow spheres, and the UiO MOFs frameworks are represented with a ball and stick model (Zr, light blue; C, grey; O, red, H, white).

Average snapshots for H<sub>2</sub>S/CH<sub>4</sub> gas mixture in UiO MOFs at 303 K and pressure from 0.5 MPa to 10 MPa are shown in Figure 6. The density distributions do not show any evident segregation between the two components.

Thaer M. Al-Jadir, and Flor R. Siperstein

\*E-mail: [150046@uotechnology.edu.iq](mailto:150046@uotechnology.edu.iq)

<https://doi.org/10.1016/j.micromeso.2018.06.002>

Microporous and Mesoporous Materials

Volume 271, 15 November 2018, Pages 160-168

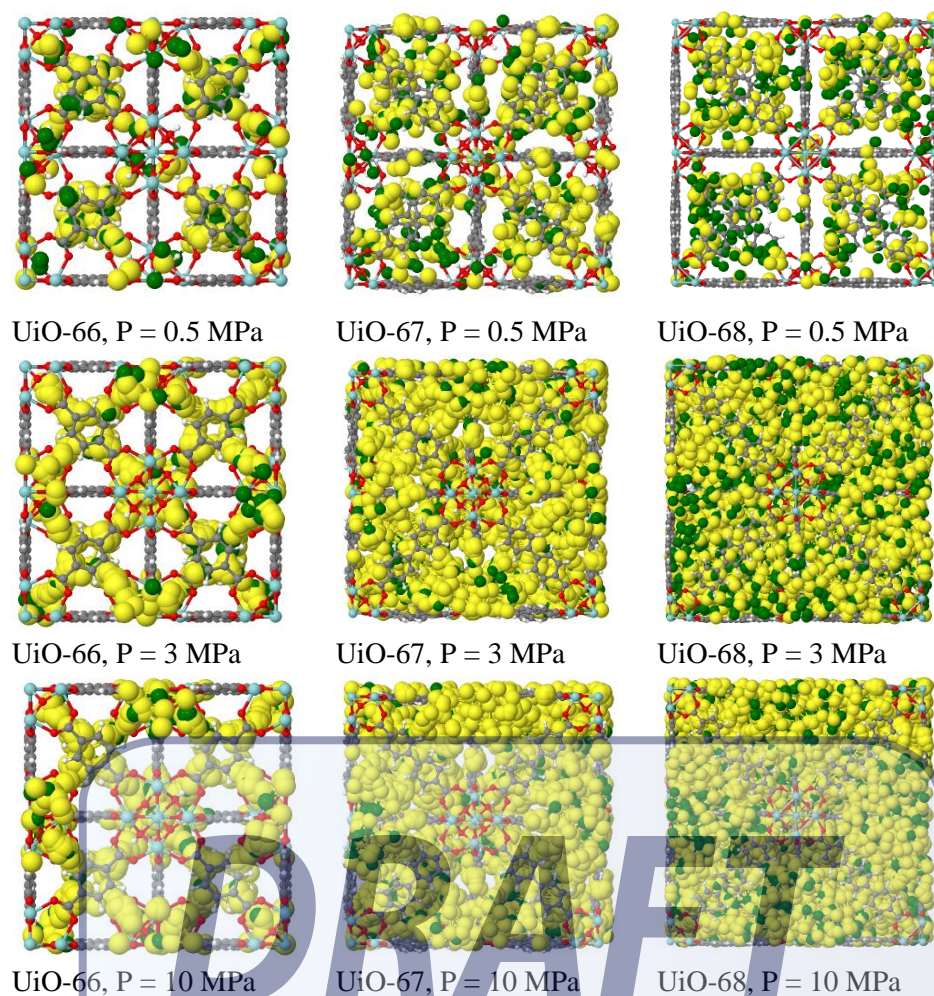


Figure 6. Location of H<sub>2</sub>S and CH<sub>4</sub> (green spheres) during simulations at different pressures and 303 K in the MOFs studied. The positions of H<sub>2</sub>S molecules during the simulation are shown as yellow spheres, the positions of CH<sub>4</sub> molecules during the simulation are shown as green spheres, and the UiO MOFs frameworks are represented with a ball and stick model (Zr, light blue; C, grey; O, red, H, white).

The radial distribution function (RDF) provides a quantitative description of the local environment of each molecule or atom in the simulation. In this work we are interested in the interactions between the adsorbed molecules and the linker. We have labelled the different carbons in the linkers to identify the difference in adsorption sites between the two molecules: the first region corresponds to the carbon atoms that connect the linker to the metal cluster (see C1 in Figure 7), the second region corresponds to carbon atoms that connect the aromatic rings (see C2, C5, C6 in Figure 7) and the third region corresponds to carbon atoms that are on the sides of the aromatic rings (see C3, C4, C7 in Figure 7).

Thaer M. Al-Jadir, and Flor R. Siperstein

\*E-mail: [150046@uotechnology.edu.iq](mailto:150046@uotechnology.edu.iq)

<https://doi.org/10.1016/j.micromeso.2018.06.002>

Microporous and Mesoporous Materials

Volume 271, 15 November 2018, Pages 160-168

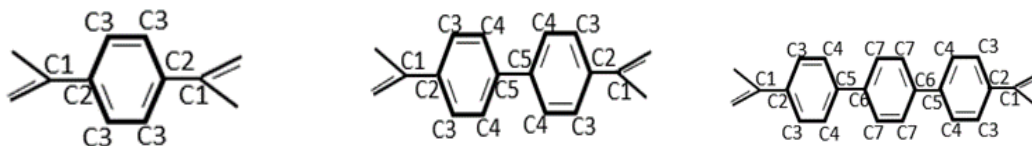
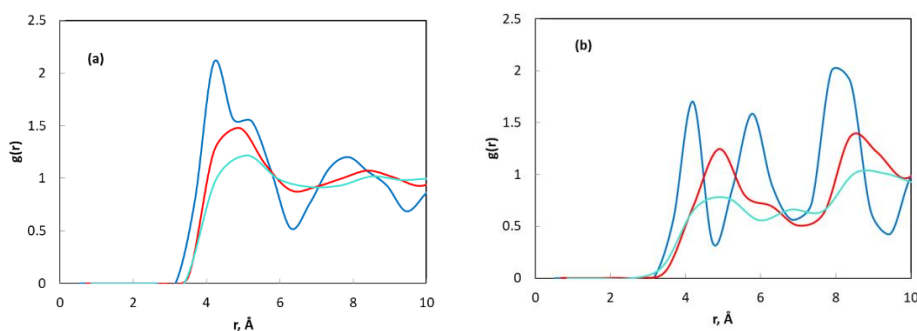


Figure 7. Schematic representation of the different carbon atoms used for the calculation of the RDFs. Region 1 corresponds to C1 atoms, region 2 corresponds to C2, C5 and C6 atoms, and region 3 corresponds to C3, C4 and C7 atoms.

Figure 8 shows the RDFs between the sulphur atom in  $H_2S$  and the carbon atoms in the linkers of the MOFs studied. The overall RDF for the three regions (averaging all the carbon atoms) is shown in Figure 8a, where not much difference is observed in the first peak of the RDF of the adsorbed gas and the carbon of the linker, having all curves approximately the same height and position regardless of the pore size. The first peak in the RDF of UiO-66 has a small shoulder and a second peak can be observed at larger distances. Considering that UiO-66 has the smallest pore size, this may represent interactions between neighboring linkers. RDFs in region 1 are significantly different in the three materials studied, showing a strong periodicity for UiO-66, which is not observed in the other materials. It is also important to note that the position of the first peak in region 1 occurs at significantly shorter distances than in the other two MOFs, suggesting that adsorption in the carbons close to the metal centres is more important in UiO-66 than in the larger pore materials. RDFs in regions 2 and 3 show that molecules adsorb closer to the carbons in region 3, suggesting that adsorption takes place at the edge of the linker rather than on the surface of the aromatic rings. RDFs between the sulphur atom in  $H_2S$  and the hydrogen atoms in the MOF linker show the same trends (see supporting information), but with even less structure than the ones shown in Figure 8. A similar behavior is observed for adsorption of pure  $CH_4$  and when  $H_2S$  is in a mixture with  $CH_4$  (Figure 9 and Figure 10). It is interesting to compare the RDFs for carbons in the different regions for the mixed gases. Even though not much difference is observed for the RDFs averaged for all carbon atoms between the pure components, significant differences are observed in the mixture, especially in the first peak in region 2, where the methane RDF is depleted significantly compared to the pure component case. This suggests that region 2 is the most favorable adsorption site for  $H_2S$ , which displaces methane when in a mixture.



Thaer M. Al-Jadir, and Flor R. Siperstein

\*E-mail: [150046@uotechnology.edu.iq](mailto:150046@uotechnology.edu.iq)

<https://doi.org/10.1016/j.micromeso.2018.06.002>

Microporous and Mesoporous Materials

Volume 271, 15 November 2018, Pages 160-168

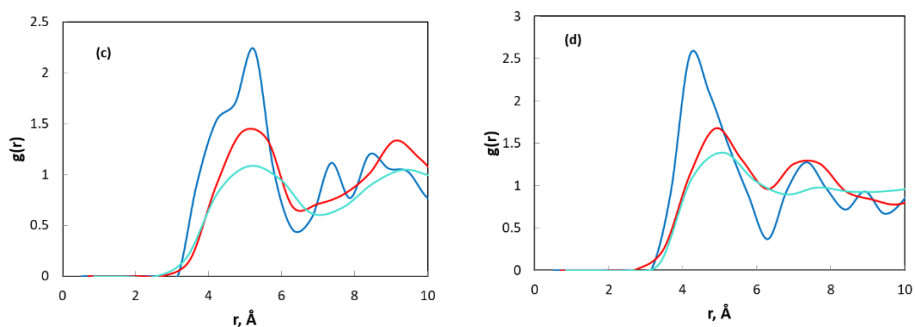


Figure 8. RDF between the sulphur atom in  $H_2S$  and the carbon atoms in the MOFs linkers for pure component simulations: (a) averaged over all carbon atoms, (b) carbon atoms in region 1, (c) carbon atoms in region 2, and (d) carbon atoms in region 3. UiO-66 is shown as a blue line, UiO-67 as a red line and UiO-68 as a turquoise line.

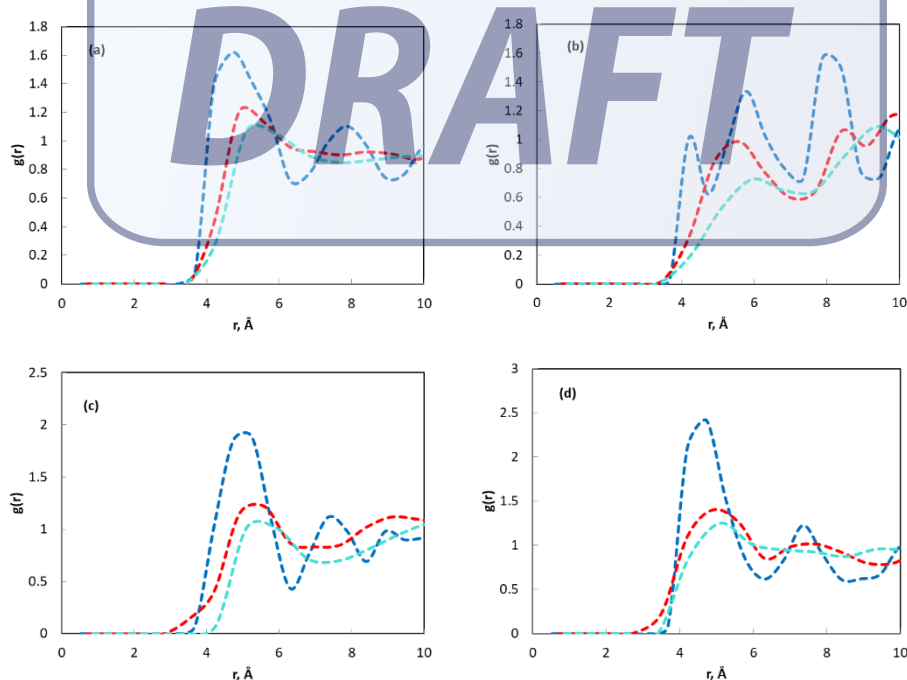


Figure 9. RDF between the carbon atom in  $CH_4$  and the carbon atoms in the MOFs linkers for pure component simulations: (a) averaged over all carbon atoms, (b) carbon atoms in region 1, (c) carbon atoms in region 2, and (d) carbon atoms in region 3. UiO-66 is shown as a blue dashed line, UiO-67 as a red dashed line and UiO-68 as a turquoise dashed line.

Thaer M. Al-Jadir, and Flor R. Siperstein

\*E-mail: [150046@uotechnology.edu.iq](mailto:150046@uotechnology.edu.iq)

<https://doi.org/10.1016/j.micromeso.2018.06.002>

Microporous and Mesoporous Materials

Volume 271, 15 November 2018, Pages 160-168

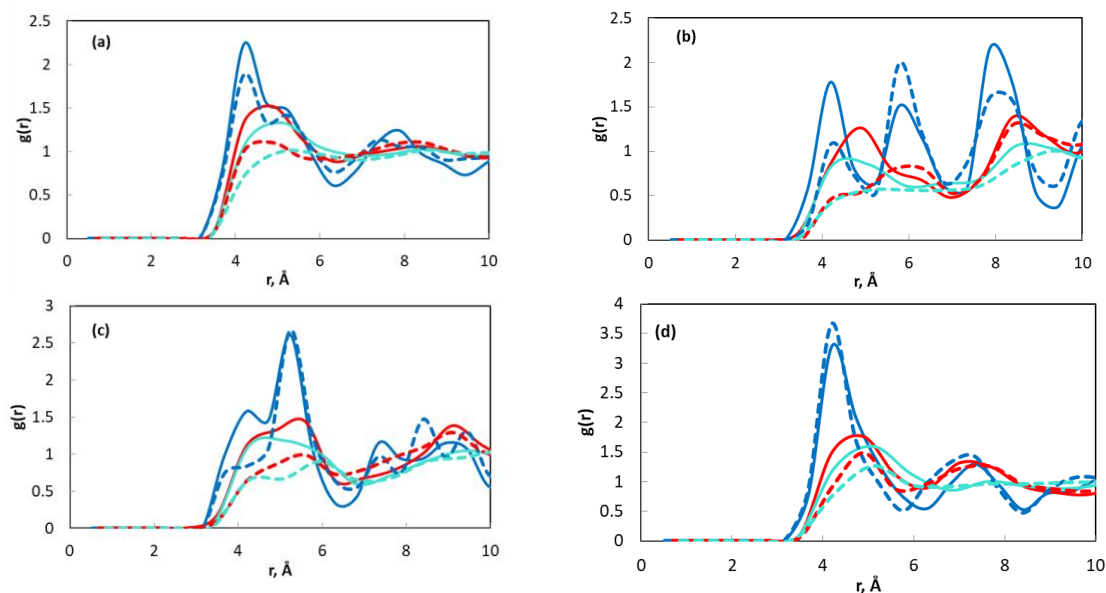


Figure 10. RDF between the sulphur atom in  $\text{H}_2\text{S}$  (solid lines) or the carbon atom in  $\text{CH}_4$  (dashed lines) and the carbon atom in the MOFs' linkers for simulations of mixtures with  $y_{\text{H}_2\text{S}} = 0.188$  at 10 MPa.: (a) averaged over all carbon atoms, (b) carbon atoms in region 1, (c) carbon atoms in region 2, and (d) carbon atoms in region 3. UiO-66 is shown as a blue line, UiO-67 as a red line and UiO-68 as a turquoise line.

## Conclusions

Based on selectivity and adsorbent selection parameter, UiO-67 MOFs has the largest potential for adsorption of hydrogen sulphide from natural gas. Extending linkers in UiO MOFs leads to a reduction in the strength of the interaction between  $\text{H}_2\text{S}$  and the MOFs. At low pressure,  $\text{H}_2\text{S}$  molecules are preferentially adsorbed in the tetrahedral cages, with increasing pressure some adsorbate molecules are pushed to the octahedral cages.

RDFs show that the adsorption takes place at the edge of the linker rather than on the surface of the aromatic rings. The second region in the linkers is the most favorable adsorption site for  $\text{H}_2\text{S}$ , which displaces methane when in a mixture.

At low pressures, the effect of the linker length is negligible as the position and height of the first peak in the RDFs is similar for all materials. Nevertheless, at high pressures the effect of the linker size becomes evident, mainly due to the larger capacity of the adsorbent when larger linkers are used, and the depletion in the height of the first peak in the RDF.

This work also shows that there is a small effect of the gas phase composition on selectivity, and more importantly, that the selectivity increases with pressure. Nevertheless, it should be kept in mind that the selectivity calculated is absolute, and in large pore materials at high pressures, excess selectivities may be different than absolute selectivities.

## Acknowledgements

Thaer M. Al-Jadir, and Flor R. Siperstein

\*E-mail: [150046@uotechnology.edu.iq](mailto:150046@uotechnology.edu.iq)

<https://doi.org/10.1016/j.micromeso.2018.06.002>

Microporous and Mesoporous Materials

Volume 271, 15 November 2018, Pages 160-168

Mr. T.M.AL.-Jadir. is grateful to the Higher Committee for Education Development in Iraq for a postgraduate research scholarship.

## References

- [1] T. Ghosh and M. Prelas, *Energy Resources and Systems*, vol. 1. Springer Netherlands, 2009.
- [2] S. Faramawy, T. Zaki, and A. A. Sakr, "Natural gas origin , composition , and processing : A review," *J. Nat. Gas Sci. Eng.*, vol. 34, pp. 34–54, 2016.
- [3] J. Carroll, *Acid Gas Injection and Carbon Dioxide Sequestration*. John Wiley & Sons, 2010.
- [4] E. Chabanon, B. Belaissaoui, and E. Favre, "Gas–liquid separation processes based on physical solvents: opportunities for membranes," *J. Memb. Sci.*, vol. 459, pp. 52–61, Jun. 2014.
- [5] F. Karadas, M. Atilhan, and S. Aparicio, "Review on the Use of Ionic Liquids (ILs) as Alternative Fluids for CO<sub>2</sub> Capture and Natural Gas Sweetening," *Energy & Fuels*, vol. 24, no. 11, pp. 5817–5828, Nov. 2010.
- [6] J. Wang and W. Zhang, "Oxidative Absorption of Hydrogen Sulfide by Iron-Containing Ionic Liquids," *Energy & Fuels*, pp. 2–7, 2014.
- [7] E. Bouhelec Blanchon le, P. Mougin, A. Barreau, and R. Solimando, "Rigorous Modeling of the Acid Gas Heat of Absorption in Alkanolamine Solutions," *Energy & Fuels*, vol. 21, pp. 2044–2055, 2007.
- [8] A. Kohl and R. Nielsen, *Gas Purification*, 5th ed. Gulf Publishing Company, 1997.
- [9] Y. Zhang, J. Sunarso, S. Liu, and R. Wang, "Current status and development of membranes for CO<sub>2</sub>/CH<sub>4</sub> separation : A review," *Int. J. Greenh. Gas Control*, vol. 12, pp. 84–107, 2013.
- [10] L. Sigot, M. Fontseré Obis, H. Benbelkacem, P. Germain, and G. Ducom, "Comparing the performance of a 13X zeolite and an impregnated activated carbon for H<sub>2</sub>S removal from biogas to fuel an SOFC : Influence of water," *ScienceDirect*, vol. 1, pp. 2–10, 2016.
- [11] A. J. Cruz, J. Pires, A. P. Carvalho, and M. B. De Carvalho, "Physical adsorption of H<sub>2</sub>S related to the conservation of works of art: The role of the pore structure at low relative pressure," *Adsorption*, vol. 11, pp. 569–576, 2005.
- [12] M. S. Shah, M. Tsapatsis, and J. I. Siepmann, "Monte Carlo simulations probing the adsorptive separation of hydrogen sulfide/methane mixtures using all-silica zeolites," *Langmuir*, vol. 31, pp. 12268–12278, 2015.
- [13] H. Maghsoudi, M. Soltanieh, H. Bozorgzadeh, and A. Mohamadalizadeh, "Adsorption isotherms and ideal selectivities of hydrogen sulfide and carbon dioxide over methane for the Si-CHA zeolite: Comparison of carbon dioxide and methane adsorption with the all-silica DD3R zeolite," *Adsorption*, vol. 19, pp. 1045–1053, 2013.
- [14] Hamon, L.; Serre, C.; Devic, T.; Loiseau, T.; Millange, F.; Férey, G.; de Weireld, G., "Comparative

Thaer M. Al-Jadir, and Flor R. Siperstein

\*E-mail: [150046@uotechnology.edu.iq](mailto:150046@uotechnology.edu.iq)

<https://doi.org/10.1016/j.micromeso.2018.06.002>

Microporous and Mesoporous Materials

Volume 271, 15 November 2018, Pages 160-168

- Study of Hydrogen Sulfide Adsorption in the MIL-53 ( Al , Cr , Fe ), MIL-47 ( V ), MIL-100 ( Cr ), and MIL-101 ( Cr ) Metal - Organic Frameworks at Room Temperature," *JACS*, vol. 53, pp. 8775–8777, 2009.
- [15] S. Vaesen, V. Guillerm, Q. Yang, A. D. Wiersum, B. Marszalek, B. Gil, A. Vimont, M. Daturi, T. Devic, P. L. Llewellyn, C. Serre, G. Maurin and G. de Weireld., "A robust amino-functionalized titanium(IV) based MOF for improved separation of acid gases," *Chem. Commun.*, vol. 49, no. 86, pp. 10082–10084, 2013.
- [16] Li, Z.; Liao, F.; Jiang, F.; Liu, B.; Ban, S.; Chen, G.; Sun, C.; Xiao, P.; Sun, Y., "Capture of H<sub>2</sub>S and SO<sub>2</sub> from trace sulfur containing gas mixture by functionalized UiO-66(Zr) materials: A molecular simulation study," *Fluid Phase Equilib.*, vol. 427, pp. 259–267, 2016.
- [17] R. C. Flagan and J. H. Seinfeld, *Fundamentals of Air Pollution Engineering*, vol. 1. Dover Publications Inc, 2012.
- [18] J. K. Brennan, K. T. Thomson, and K. E. Gubbins, "Adsorption of Water in Activated Carbons : Effects of Pore Blocking and Connectivity," *Langmuir*, vol. 18, pp. 5438–5447, 2002.
- [19] A. Di Lella, N. Desbiens, A. Boutin, I. Demachy, P. Ungerer, J.-P. Bellat and A. H. Fuchs., "Molecular simulation studies of water physisorption in zeolites," *Phys. Chem. Chem. Phys.*, vol. 8, pp. 5396–406, 2006.
- [20] A. M. Ebrahim, B. Levasseur, and T. J. Bandoz, "Interactions of NO<sub>2</sub> with Zr-Based MOF: Effects of the Size of Organic Linkers on NO<sub>2</sub> Adsorption at Ambient Conditions," *Langmuir*, vol. 29, 2013.
- [21] D. Fairen-jimenez, N. A. Seaton, and T. Düren, "Unusual Adsorption Behavior on Metal - Organic Frameworks," *Langmuir*, vol. 26, pp. 14694–14699, 2010.
- [22] Cavka, J. H.; Jakobsen, S.; Olsbye, U.; Guillou, N.; Lamberti, C.; Bordiga, S.; Lillerud, K. P., "A New Zirconium Inorganic Building Brick Forming Metal Organic Frameworks with Exceptional Stability," *JACS*, vol. 6, pp. 13850–13851, 2008.
- [23] N. C. Burtch, H. Jasuja, and K. S. Walton, "Water Stability and Adsorption in Metal – Organic Frameworks," *Chem. Rev.*, vol. 114, pp. 10575–10612, 2014.
- [24] G. Nickerl, M. Leistner, S. Helten, V. Bon, I. Senkovska, and S. Kaskel, "Integration of accessible secondary metal sites into MOFs for H<sub>2</sub>S removal," *Inorg. Chem. Front.*, vol. 1, no. 4, p. 325, 2014.
- [25] Y. Bai, Y. Dou, L. Xie, W. Rutledge, J. Li, and H. Zhou, "Zr-based metal–organic frameworks: design, synthesis, structure, and applications," *Chem. Soc. Rev.*, vol. 45, pp. 2327–2367, 2016.
- [26] Q. Yang, V. Guillerm, F. Ragon, A. D. Wiersum, P. L. Llewellyn, C. Zhong, T. Devic and G. Maurin, "CH<sub>4</sub> storage and CO<sub>2</sub> capture in highly porous zirconium oxide based metal–organic frameworks," *COMMUNICATION*, 2012.
- [27] L. Sarkisov and A. Harrison, "Computational structure characterisation tools in application to ordered and disordered porous materials materials," *Mol. Simul.*, vol. 7022, 2011.

Thaer M. Al-Jadir, and Flor R. Siperstein

\*E-mail: [150046@uotechnology.edu.iq](mailto:150046@uotechnology.edu.iq)

<https://doi.org/10.1016/j.micromeso.2018.06.002>

Microporous and Mesoporous Materials

Volume 271, 15 November 2018, Pages 160–168

- [28] M. G. Martin, “MCCCS Towhee: a tool for Monte Carlo molecular simulation,” *Mol. Simul.*, vol. 39, pp. 1212–1222, 2013.
- [29] G. C. A. M. Mooij, D. Frenkel, and B. Smit, “Direct simulation of phase equilibria of chain molecules,” *J. Phys. Condens. Matter*, vol. 4, pp. L255–L259, 1999.
- [30] L.-Y. Deng, “Efficient and portable multiple recursive generators of large order,” *ACM Trans. Model. Comput. Simul.*, vol. 15, pp. 1–13, 2005.
- [31] D. Frenkel and B. Smit, *Understanding Molecular Simulation: From Algorithms to Applications*. London, UK: Academic Press, 2002.
- [32] T. Darden, L. Perera, L. Li, and P. Lee, “New tricks for modelers from the crystallography toolkit: The particle mesh Ewald algorithm and its use in nucleic acid simulations,” *Structure*, vol. 7, no. 3, pp. 55–60, 1999.
- [33] S. L. Mayo, B. D. Olafson, and W. A. G. Goddard III, “DREIDING: A Generic Force Field for Molecular Simulations,” *J. Phys. Chem.*, vol. 101, pp. 8897–8909, 1990.
- [34] A. K. Rappe, C. J. Casewit, K. S. Colwell, W. A. Goddard III, and W. M. Skiff, “UFF, a Full Periodic Table Force Field for Molecular Mechanics and Molecular Dynamics Simulations,” vol. 2, pp. 10024–10035, 1992.
- [35] G. Kamath, N. Lubna, and J. J. Potoff, “Effect of partial charge parametrization on the fluid phase behavior of hydrogen sulfide,” *J. Chem. Phys.*, vol. 123, no. 12, pp. 0–7, 2005.
- [36] M. G. Martin and J. I. Siepmann, “Transferable Potentials for Phase Equilibria. 1. United-Atom Description of n -Alkanes,” *J. Phys. Chem. B*, vol. 5647, pp. 2569–2577, 1998.
- [37] C. Cai, Z. Xie, R. H. Worden, G. Hu, L. Wang, and H. He, “Methane-dominated thermochemical sulphate reduction in the Triassic Feixianguan Formation East Sichuan Basin , China : towards prediction of fatal H<sub>2</sub>S concentrations,” *Mar. Pet. Geol.*, vol. 21, pp. 1265–1279, 2004.
- [38] R. Q. Snurr, A. T. Bell, and D. N. Theodorou, “Prediction of Adsorption of Aromatic Hydrocarbons in Silicalite from Grand Canonical Monte Carlo Simulations with Biased Insertions,” *J. Phys. Chem.*, vol. 97, pp. 13742–13752, 1993.
- [39] S. U. Rege and R. T. Yang, “A simple parameter for selecting an adsorbent for gas separation by pressure swing adsorption,” *Sep. Sci. Technol.*, vol. 36, no. 15, pp. 3355–3365, 2001.
- [40] R. T. Yang, *Adsorbents: fundamentals and applications*, John Wiley & Sons, 2003.
- [41] P. L. and G. M. F. Rouquerol, J. Rouquerol, K.S.W. Sing, *Adsorption by Powders and Porous Solids Principles, Methodology and Applications*, 2nd ed. Academic Press, 2014.
- [42] . Toth, *Adsorption Theory, Modeling, and Analysis*, 1st ed. Marcel Dekker, 2002.
- [43] M. Suzuki, *Adsorption Engineering*, 1st ed. Kodansha, 1990.
- [44] A. Dąbrowski, “Adsorption — from theory to practice,” *Adv. Colloid Interface Sci.*, vol. 93, 2001.

Preprint version of : The influence of the pore size in Metal–Organic Frameworks in adsorption and separation of hydrogen sulphide: a molecular simulation study

Thaer M. Al-Jadir, and Flor R. Siperstein

\*E-mail: [150046@uotechnology.edu.iq](mailto:150046@uotechnology.edu.iq)

<https://doi.org/10.1016/j.micromeso.2018.06.002>

Microporous and Mesoporous Materials

Volume 271, 15 November 2018, Pages 160-168